Supporting Information for

Mass-amplifying electrochemiluminescence film (MAEF) for visual detection of dopamine in aqueous media

Zihua Li, Wei Qin, and Guodong Liang*

PCFM lab, School of Materials Science and Engineering, Sun Yat-sen University, Guangzhou, 510275, China.

* Corresponding author: E-mail address: lgdong@mail.sysu.edu.cn (G. L.)

Table of Contents

1. Materials and instruments

1.1 Chemicals

4,7-dibromo-2,1,3-benzothiadiazole, 4-(diphenylamino)phenylboronic acid, potassium carbonate, tetrahydrofuran, tetrakis(triphenylphosphine)palladium, dichloromethane, toluene, cyclohexane, *N*,*N*-Dimethylformamide and tetrabutylammonium hexafluorophosphate were purchased from Energy Chemical or Soochiral Chemical Science & Technology in China. Dopamine hydrochloride, ascorbic acid, uric acid, gulcose, TEOA, DBAE, TPrA, $Na_2C_2O_4$ and Na_2SO_4 were purchased from Macklin. Gold, copper, and type 304 stainless steel wafers were obtained from Aidahengsheng (Tianjin, China). ITO wafers were purchased from Shenzhen Laibao Hi-Tech Co., Ltd. Glassy carbon electrode (GCE) was obtained from Chenhua instrument (China). Phosphate buffer solutions were prepared by mixing balanced amounts of 0.2 M Na_2HPO_4 and NaH_2PO_4. All regents or chemicals were used as received without any further purification.

1.2 Preparation of BTD-TPA films

The BTD-TPA films were facilely prepared by drop-casting 5 μL of DCM solution of BTD-TPA on different electrodes, allowing it to air dry. The film thickness is controlled by dropping BTD-TPA solutions with different concentrations on the electrode surface.

1.3 Characterizations

The NMR spectra were measured on a Bruker AV 400 spectrometer in $CDCl_3$ with tetramethylsilane (TMS) as internal reference. The high-resolution mass spectra (HRMS) were recorded using a mass spectrometer (LTQ XL, ThermoFisher, America) operating in matrix-assisted laser desorption ionization time-of-flight (MALDI-TOF) mode. UV-vis absorbance spectra were recorded with a SOPTOP 752 spectrometer. PL spectra were measured on a GANGDONG F-380 spectrofluorometer. Fluorescent lifetime was recorded on an LTD FLSP 920 spectrometer (Edinburgh Instruments, UK). Quantum yield of BTD-TPA in solid powder was recorded by using an Edinburgh Instruments

spectrometer (FLSP920) with a calibrated integrating sphere. The morphologies of BTD-TPA films were characterized by scanning electron microscopy (SEM, Quanta 400, FEI Company). Transmission electron microscopy (TEM) was carried out using a transmission electron microscope (JEOL, JEM-2010F) operated at an acceleration voltage of 200 kV. The X-ray diffraction (XRD) pattern was recorded on an X-ray diffractometer (XRD, D8 Advance, Bruker) with Cu Ka radiation. The thickness of BTD-TPA films measured using a profilometer (Ambios XP-1, Ambios Technology Inc.). The fluorescence images of BTD-TPA single crystal and films were measured by a fluorescence microscope instrument (LEICA M205 FA). All the optical photos of ECL and PL were recorded using a commercial mobile phone camera (HUAWEI P30).

1.4 Electrochemical and ECL measurements

All electrochemistry experiments were performed with a three-electrode cell on an electrochemical work station (CHI 660D, Chenhua instrument, China). Au, Cu and type 304 stainless steel wafers (1×1 cm^2), GCE (3 mm diameter) and ITO (2×2 cm^2) were employed as the working electrodes. Platinum wire was used as the counter electrode and Ag/AgCl was served as the reference electrode. Before usage, all working electrodes were polished with 0.5, 0.3, and 0.05 μm alumina powder dispersed in water and sonicated in ethanol and deionized water. A photomultiplier tube detector (PMT, Hamamatsu, Japan) with the voltage at 800V was employed to collect the ECL signal. The ECL spectrum was obtained *via* pulsing 80 mV past the peak potentials of the oxidation waves for BTD-TPA with a pulse width of 1 s by differential pulse amperometry. The ECL stability profile was obtained by plusing between 80 mV past the oxidation peak and 0 V for BTD-TPA by means of multi-potential steps, with a pulse width of 2 s.

1.5 Density functional theory (DFT) calculations

Optimized geometries and molecular orbitals of HOMO and LUMO levels of BTD-TPA, *p*-benzoquinone and oxidized species of DA were calculated using a density functional theory (DFT) method (B3LYP/6-31+(d) of the optimized structures; Gaussian 09).

2. Synthesis of BTD-TPA

The compound was synthesized by following the procedure reported in literature [1]. A mixture of 4,7-dibromo-2,1,3-benzothiadiazole (147 mg, 0.5 mmol), 4-(diphenylamino)phenylboronic acid (434 mg, 1.5 mmol), $Pd(PPh_3)_4$ (50 mg, 0.04 mmol), K_2CO_3 (690 mg, 5 mmol), THF (40 mL) and water (8 mL) was heated to 60 °C for 24 h under nitrogen and stirring. The mixture was cooled to room temperature. The solvents were removed under reduced pressure. Dichloromethane (150 mL) and water (50 mL) were added. The organic layer was separated and washed with water (150 mL) three times, dried over anhydrous Na_2SO_4 and evaporated to dryness under reduced pressure. The crude product was purified by column chromatography on silica gel using hexane/dichloromethane as eluent. Yield: 52%. ^{1}H NMR (400 MHz, $CDCl_3$) δ (ppm): 7.06 (t, 2H, Ar H), 7.20 (t, 12H, Ar H), 7.29 (t, 8H, Ar H), 7.74 (t, 2H, Ar H), 7.88 (d, 4H, Ar H); ^{13}C NMR (125 MHz, $CDCl_3$) δ (ppm): 123.3, 124.9, 127.4, 129.4, 129.9, 131.0, 132.2, 147.5, 148.0, 154.2; HRMS (MALDI-TOF) *m*/*z*: [M^+] calcd for $C_{42}H_{30}N_4S$, 622.2191; found, 622.1989.

3. Supplementary figures

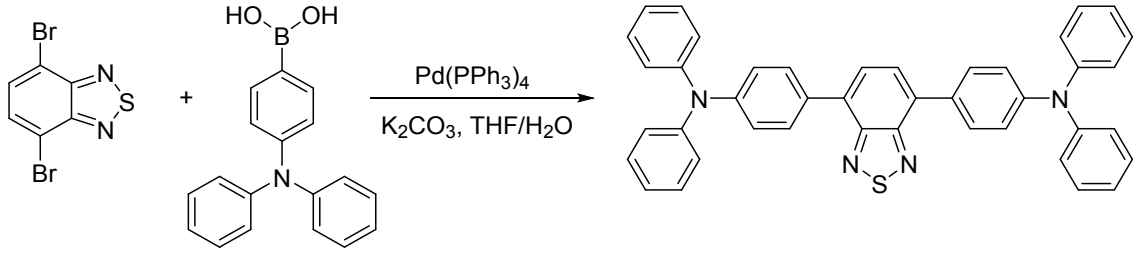

Scheme S1 Synthetic route for BTD-TPA.

BTD-TPA was facilely synthesized through a one-step Suzuki coupling reaction with a high yield (Scheme S1). It is soluble in common organic solvents such as tetrahydrofuran (THF) and dichloromethane (DCM), but insoluble in water. Red-shifted fluorescence with increasing solvent polarity and density functional theory (DFT) calculations of BTD-TPA (Fig. S1 and S2) indicate strong charge transfer effects from electron-donating triphenylamine (TPA) wings to the electron-withdrawing BTD core. Cyclic voltammograms (CV) of BTD-TPA show a stable and reversible redox pair at +1.1 V due to the presence of arylamine moieties (Fig. S3). The i_{pa}/i_{pc} value is close to unity, revealing that radical cations produced during anodic potential scanning are stable [2].

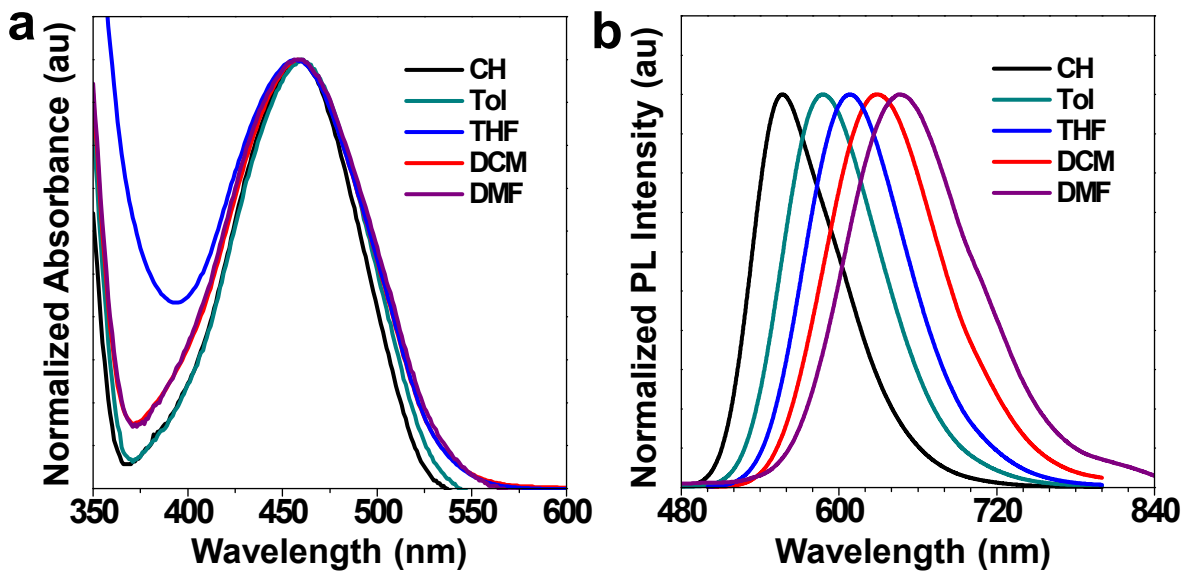

Fig. S1 Normalized UV-vis (a) and photoluminescence (PL) (b) spectra of BTD-TPA in solvents with different polarities including cyclohexane (CH), toluene (Tol), tetrahydrofuran (THF), dichloromethane (DCM), N, N-dimethylformamide (DMF). Compound concentration: 10 μM.

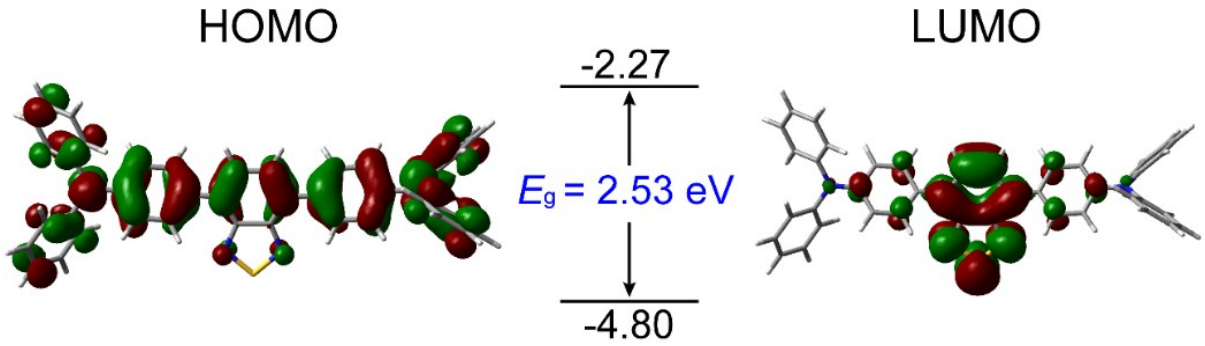

Fig. S2 Optimized geometries and molecular orbitals of HOMO and LUMO levels of BTD-TPA.

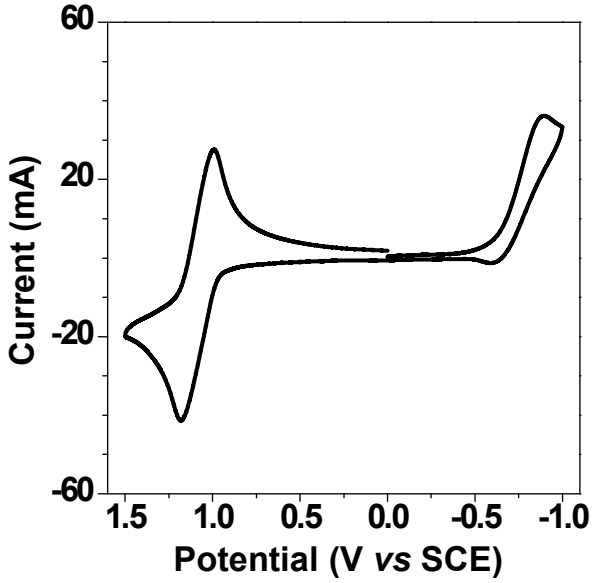

Fig. S3 CV of BTD-TPA in anhydrous DCM containing 0.1M $TBAPF_6$. Scan rate: 0.1V/s. Compound concentration: 1mM.

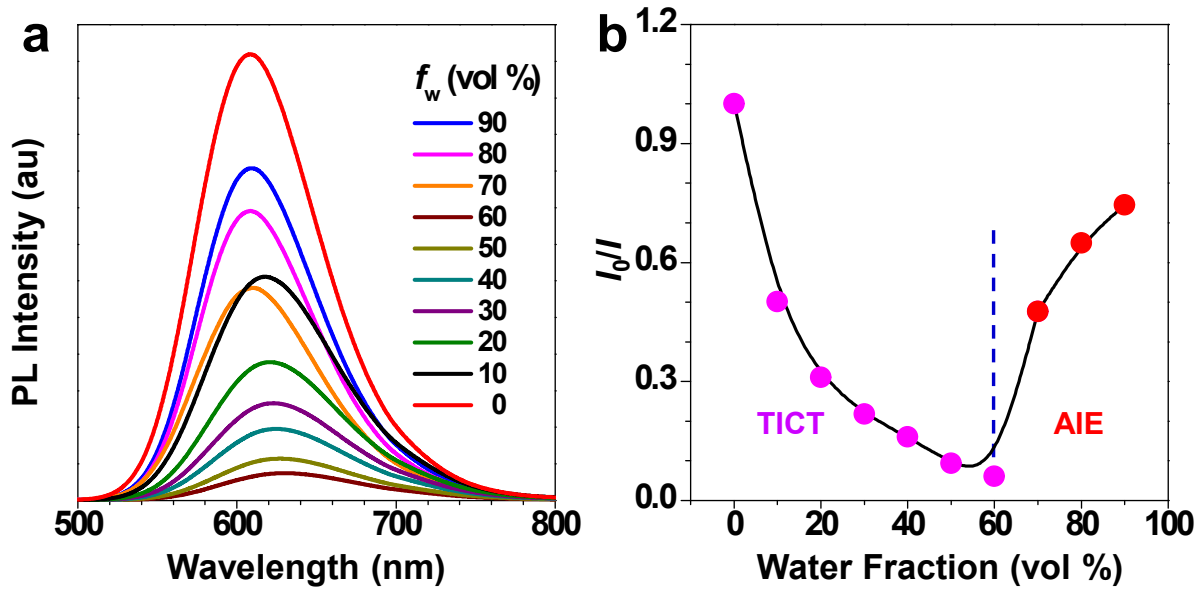

Fig. S4 (a) Photoluminescence (PL) spectra and (b) the plot of relative PL intensity (I/I_0) of BTD-TPA versus water fraction (f_w) in THF/water mixtures. I_0: emission intensity in pure THF. Compound concentration: 10 μM; λ_{ex} = 460 nm.

To study the effect of aggregation on its emission process, the photoluminescence (PL) spectra of the luminogen were explored in THF/water mixtures with different water fractions (f_w). As shown in Fig. S4, the luminogen in pure THF emits orange-red fluorescence with an emission maximum at 609 nm. With gradual addition of water into THF ($f_w \leq 60\%$), the emission is weakened and red-shifted to *ca.* 625 nm due to twisted intramolecular charge transfer (TICT) in polar solvent mixtures [3]. The mixture is transparent without formation of aggregates at $f_w \leq 60\%$. Afterwards ($f_w > 70\%$), the mixture becomes turbid, and PL intensity starts to increase due to the AIE effect from the freely rotating rotors of arylamino units. The higher the water fraction, the stronger the emission intensity. At f_w = 90%, PL intensity recovers remarkably, and the emission maximum moves to 609 nm.

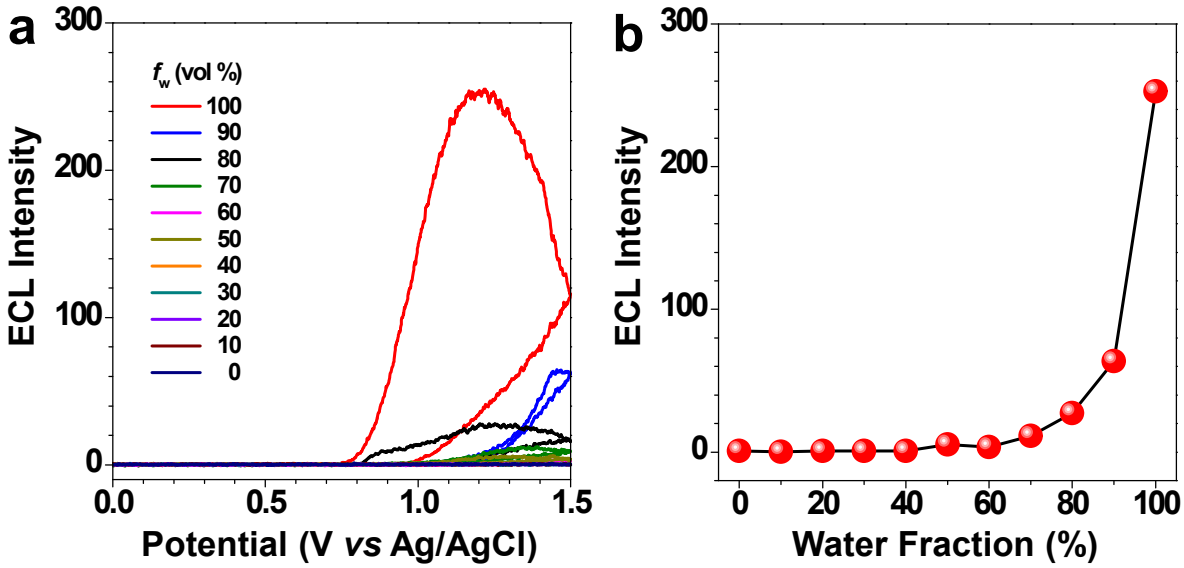

Fig. S5 (a) ECL intensity-potential profiles, and (b) ECL intensity plots of the film on GCE as a function of water fraction in THF/H_2O mixed solvent. Luminogen loading was 600 ng/mm^2.

It is noted that PL intensity of BTD-TPA is strongest in pure THF (Fig. S4), while ECL signal is not detected in pure THF solutions using glassy carbon (Fig. S5). PL spectra of BTD-TPA/THF solution are excited by UV light at 350 nm. Most of luminogen molecules are excited and involved in light emission, leading to strong PL intensity. In contrast, ECL of BTD-TPA/THF solution is triggered by electrochemical reactions near the electrode surface. Luminogen concentration near electrode surface is low in BTD-TPA/THF solution, leading to low concentration of excited luminogen molecules and faint ECL.

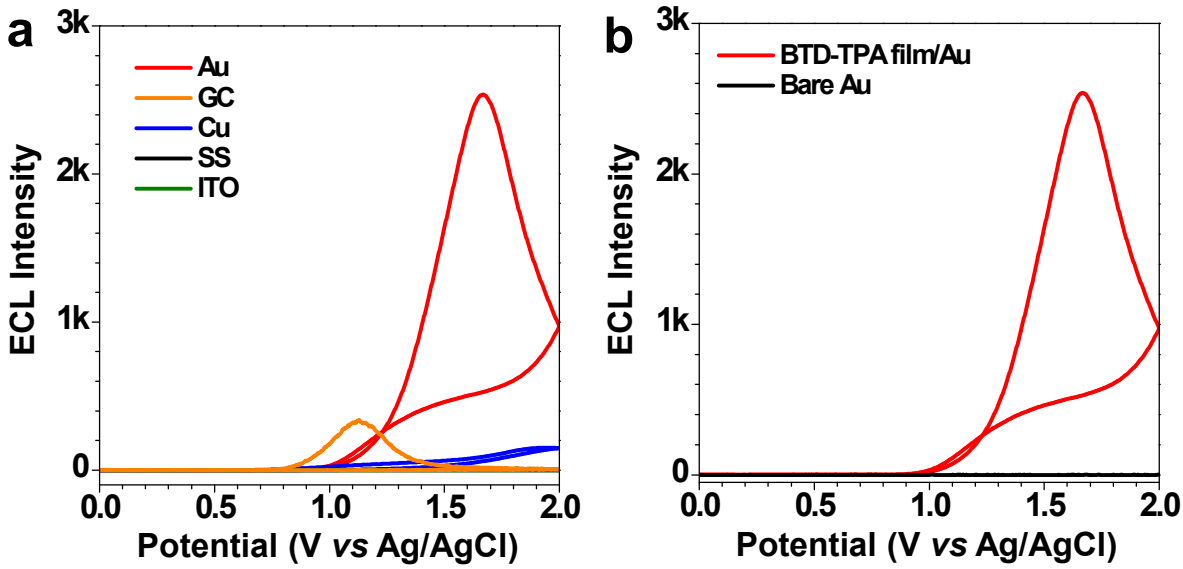

Fig. S6 (a) ECL intensity profiles of the BTD-TPA film on different electrodes in PBS solutions. (b) ECL intensity of the BTD-TPA film on Au wafers and bare Au wafers in identical conditions. Luminogen loading was 260 ng/mm^2.

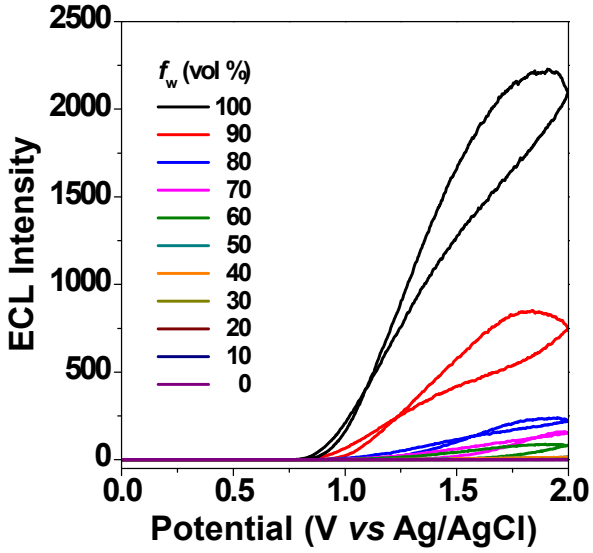

Fig. S7 ECL intensity-potential profiles of the BTD-TPA film on Au wafers as a function of water fraction in THF/H_2O mixed solvent. Luminogen loading was 520 ng/mm^2.

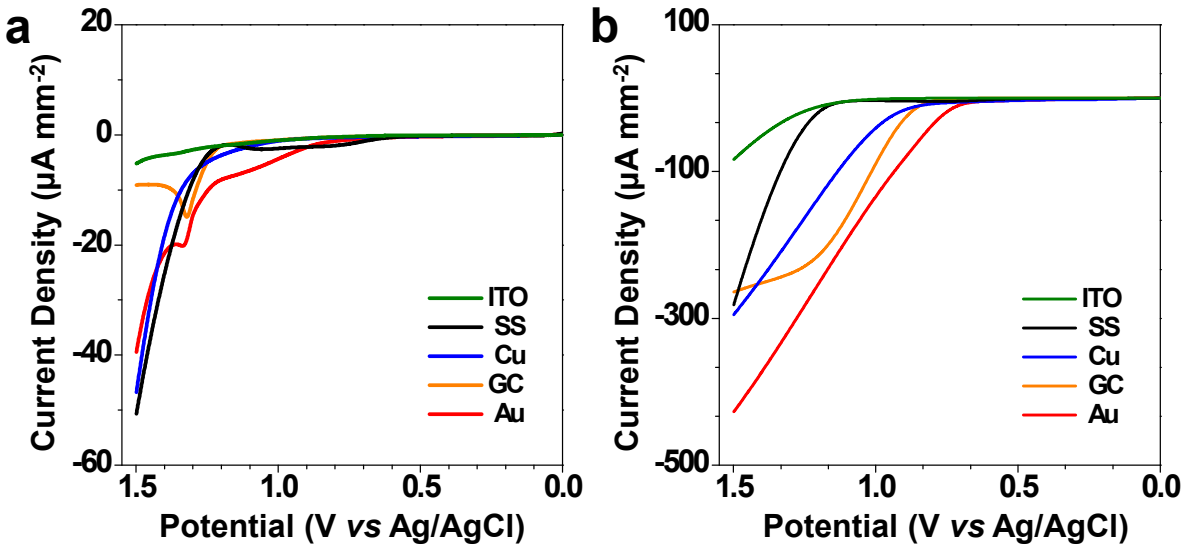

Fig. S8 LSV curves of (a) BTD-TPA films on different electrodes and (b) TEOA (300 mM) in 0.2 M PBS solutions. pH = 8. Luminogen loading was 520 ng/mm^2.

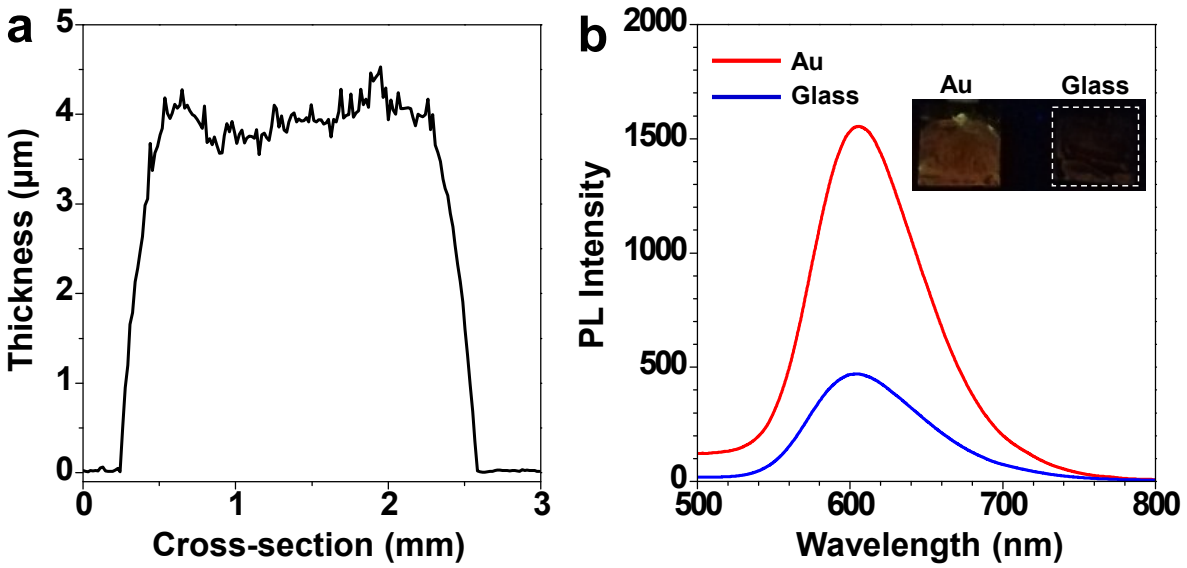

Fig. S9 (a) Profilometry traces for BTD-TPA films at loadings of 520 ng/mm^2 with a thickness of 3.67 um. (b) PL spectra of BTD-TPA films on Au and glass wafers. λ_{ex} = 460 nm.

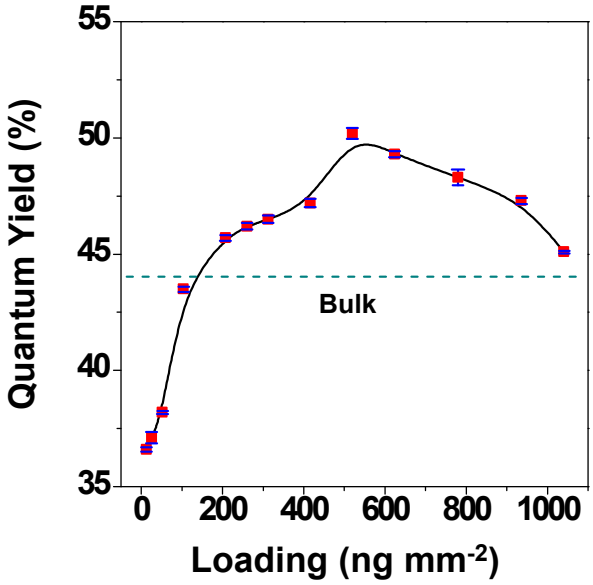

Fig. S10 Fluorescence quantum yields of BTD-TPA films on Au wafers at various loadings.

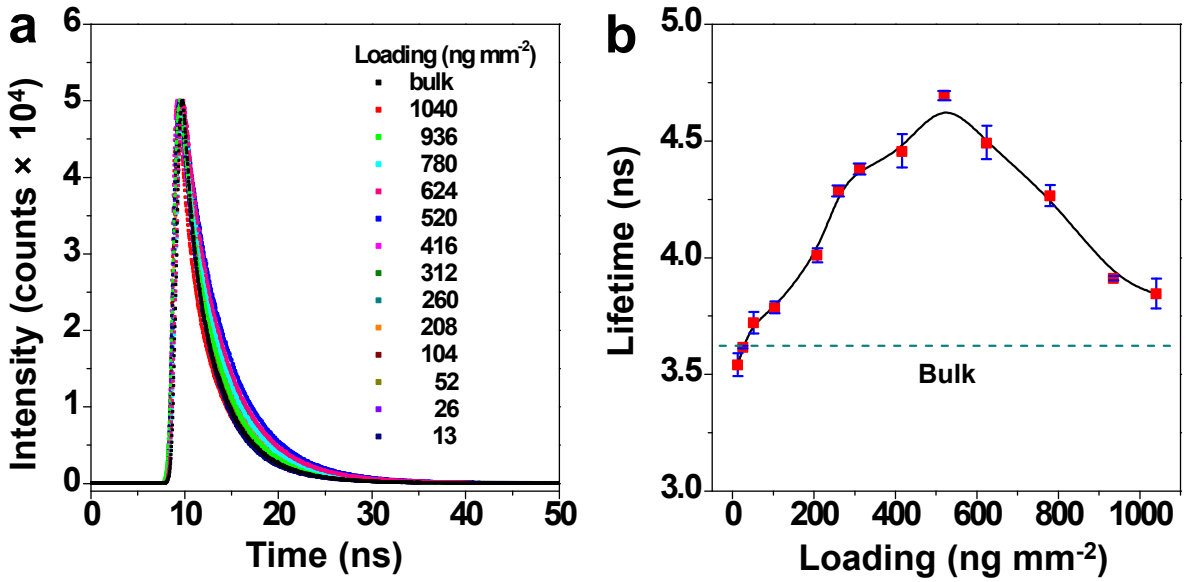

Fig. S11 (a) Time-resolved photoluminescence spectra, and (b) lifetime of BTD-TPA film on Au wafers at various loadings. λ_{ex} = 460 nm.

Calculation of radiative and non-radiative decay rate constants.

Fluorescence typically follows first-order kinetics:

$$[S] = [S]_0 e^{-t/\tau} \quad \text{(S1)}$$

[S] is the concentration of exited state molecules at time t, $[S]_0$ is the initial concentration and τ is the fluorescence lifetime.

Decay rate (k) is the inverse of lifetime, consisting of radiative and non-radiative decay rate constants:

$$k = k_{rad} + k_{nrad} \quad \text{(S2)}$$

where k_{rad} is the radiative decay rate constant and k_{nrad} is the non-radiative decay rate constant. The quantum yield (Φ) is defined as the fraction of emission process in which emission of light is involved:

$$\Phi = \frac{k_{rad}}{k_{rad} + k_{nrad}} \quad \text{(S3)}$$

The values of radiative and non-radiative rate constants of the film were tabulated in Table 1.

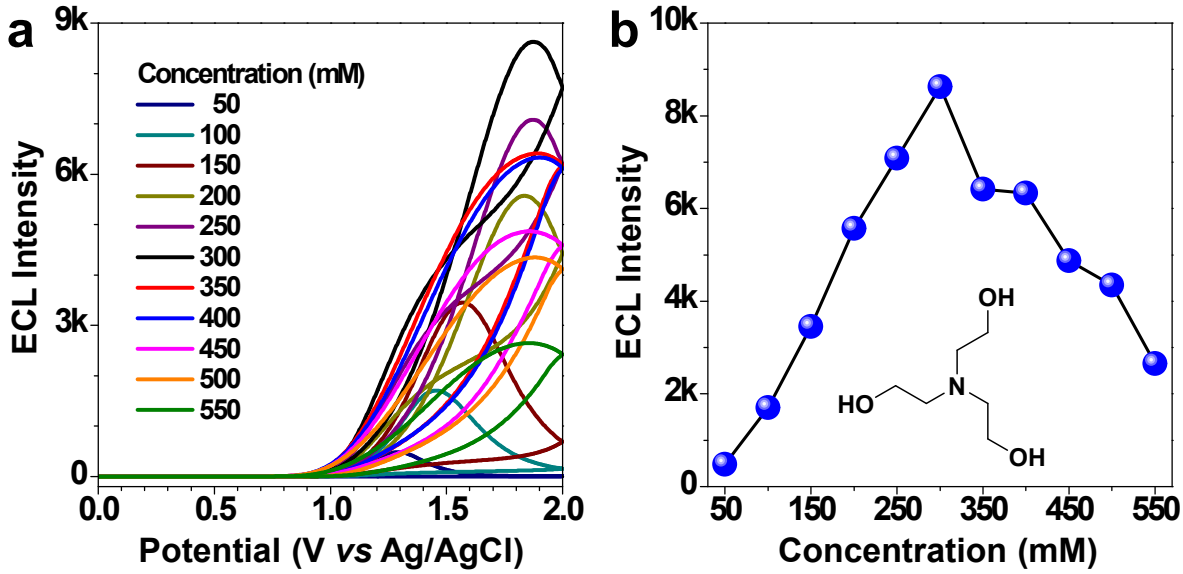

Fig. S12 (a) ECL intensity-potential profiles of BTD-TPA films on Au electrodes in 0.2 M PBS solutions containing various amounts of TEOA and (b) the plots of the maximum ECL intensity against TEOA concentration. pH= 8. Luminogen loading was 520 ng/mm^2.

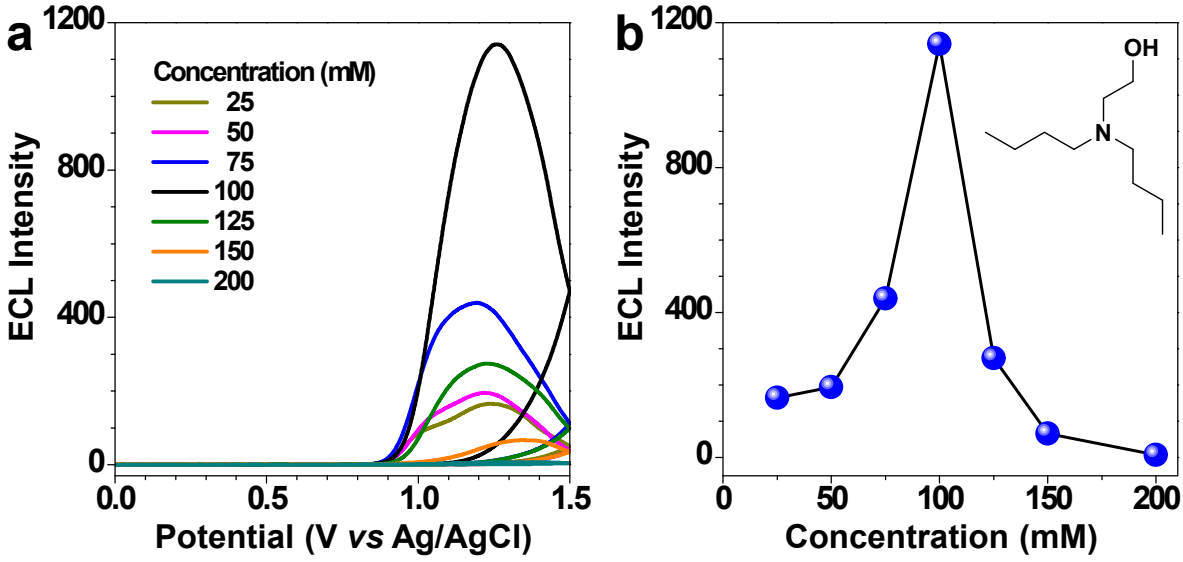

Fig. S13 (a) ECL intensity-potential profiles of BTD-TPA films on Au electrodes in 0.2 M PBS solutions containing various amounts of DBAE and (b) the plots of the maximum ECL intensity against DBAE concentration. pH= 8. Luminogen loading was 520 ng/mm^2.

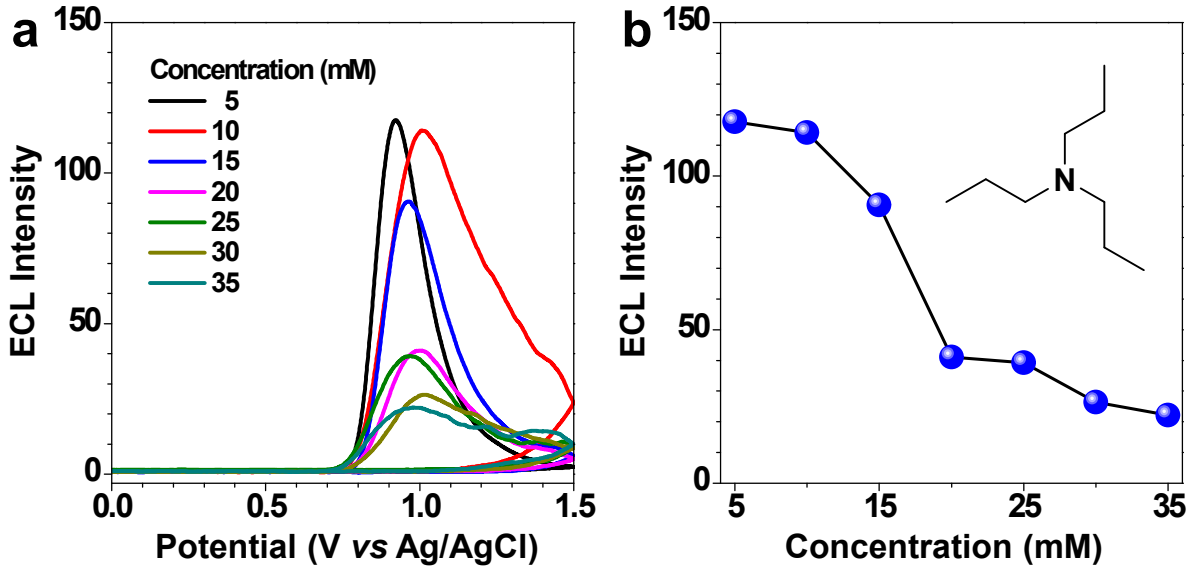

Fig. S14 (a) ECL intensity-potential profiles of BTD-TPA films on Au electrodes in 0.2 M PBS solutions containing various amounts of TPrA and (b) the plots of the maximum ECL intensity against TPrA concentration. pH= 8. Luminogen loading was 520 ng/mm^2.

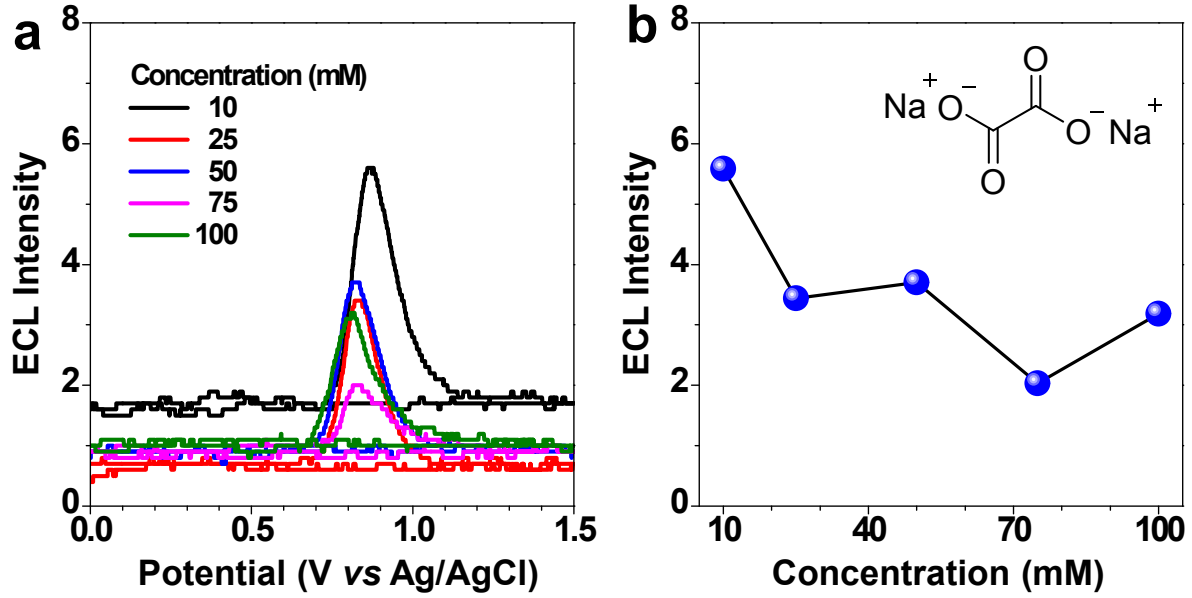

Fig. S15 (a) ECL intensity-potential profiles of BTD-TPA films on Au electrodes in 0.2 M PBS solutions containing various amounts of $Na_2C_2O_4$ and (b) the plots of the maximum ECL intensity against $Na_2C_2O_4$ concentration. pH= 8. Luminogen loading was 520 ng/mm^2.

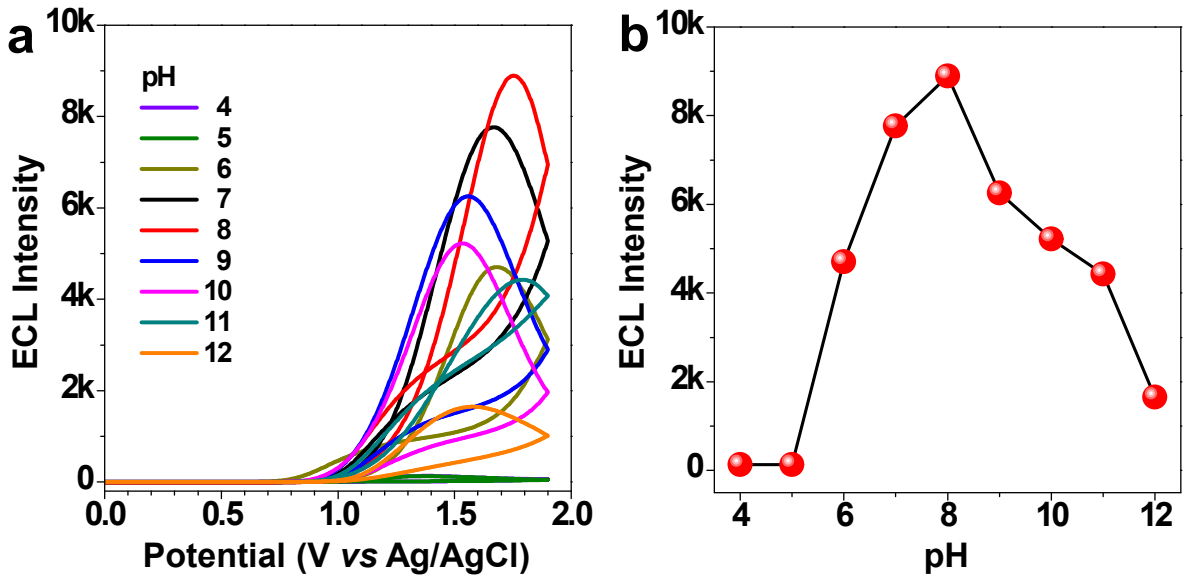

Fig. S16 (a) ECL intensity-potential profiles of BTD-TPA films on Au electrodes in 0.2 M PBS solutions at various pH and (b) the plots of the maximum ECL intensity against pH value. TEOA: 300 mM. Luminogen loading was 520 ng/mm^2.

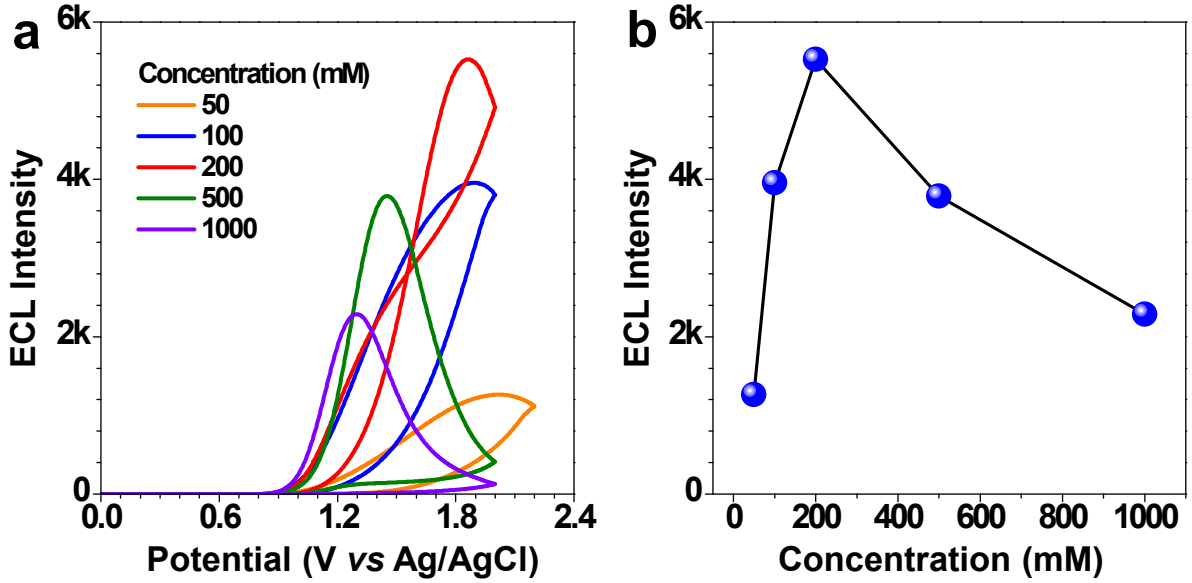

Fig. S17 (a) ECL intensity-potential profiles of BTD-TPA films on Au electrodes in PBS solutions at different concentrations and (b) the plots of the maximum ECL intensity against PBS concentration. pH= 8. Luminogen loading was 520 ng/mm^2.

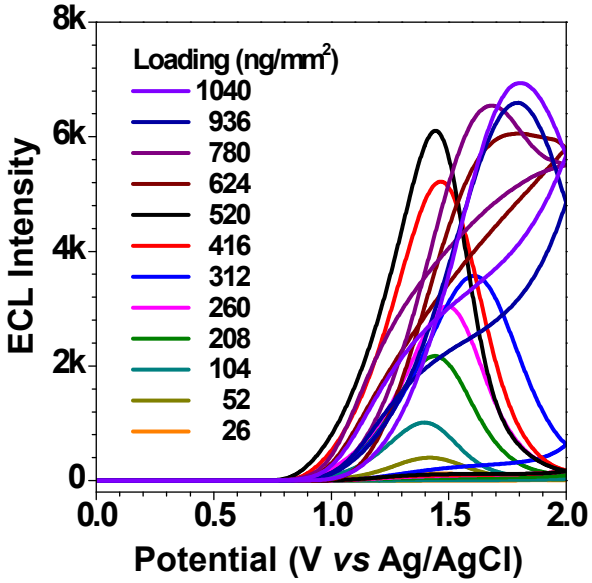

Fig. S18 ECL intensity-potential profiles of BTD-TPA films on Au electrodes at various loadings.

Calculation of the ECL efficiency

The ECL efficiency refers to its relative ECL efficiency compared with the ECL system of ($Ru(bpy)_3^{2+}$/TprA) by integration of both ECL intensity and current value versus time, and is calculated through the following equation [4,5]:

$$\Phi_{ECL} = \Phi_{ECL,\,st} \times \left[\frac{\int_a^b ECLdt}{\int_a^b Currentdt}\right]_x \Big/ \left[\frac{\int_a^b ECLdt}{\int_a^b Currentdt}\right]_{st}$$

where Φ_{ECL}, *x*,and *st* represent ECL efficiency, BTD-TPA and $Ru(bpy)_3^{2+}$, respectively. $\Phi_{ECL,st}$ value is set to 1 as the standard from the measurable ECL emission of 1mM $Ru(bpy)_3^{2+}$ in 0.2 M PBS solution (pH = 8) with 0.1 M TprA at +1.2 V.

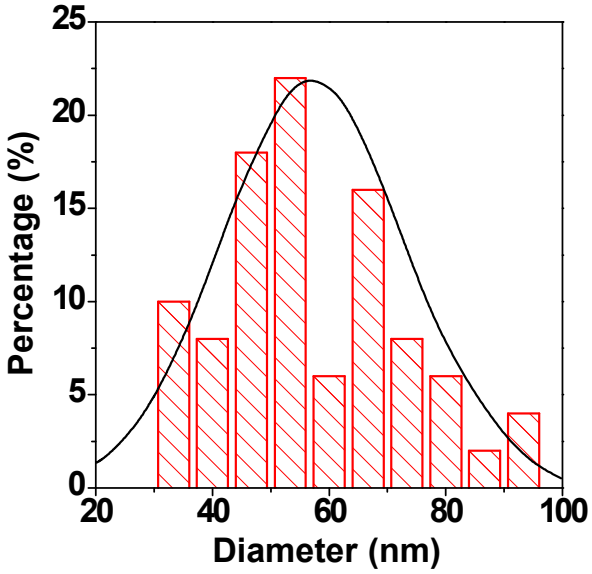

Fig. S19 Diameter distribution of BTD-TPA nanowires on gold wafers.

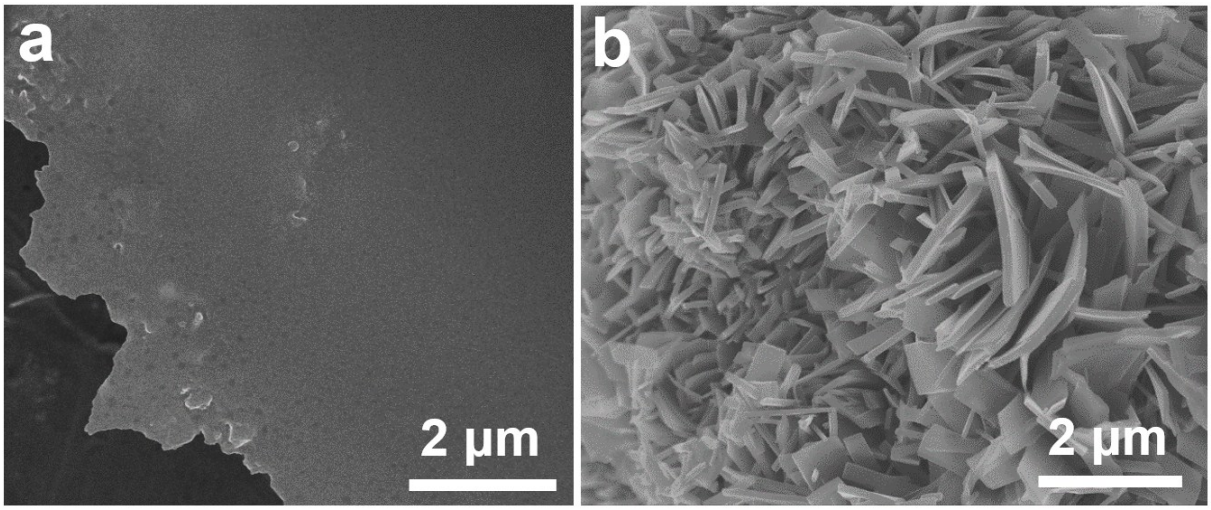

Fig. S20 SEM images of BTD-TPA films on Au wafers at different loadings. (a) 104 ng/mm^2 and (b) 312 ng/mm^2.

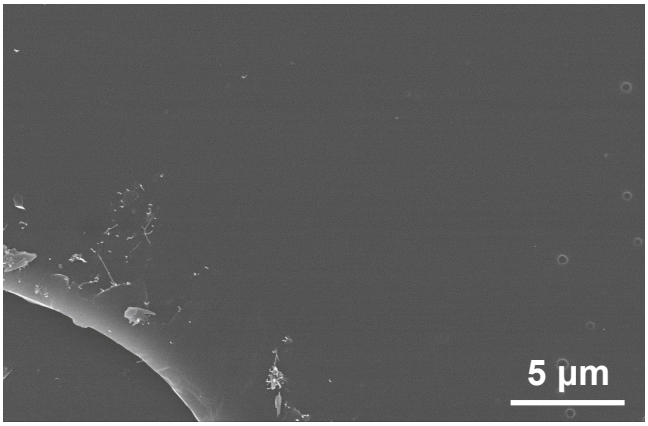

Fig. S21 SEM images of BTD-TPA films on glassy carbon electrode (GCE).

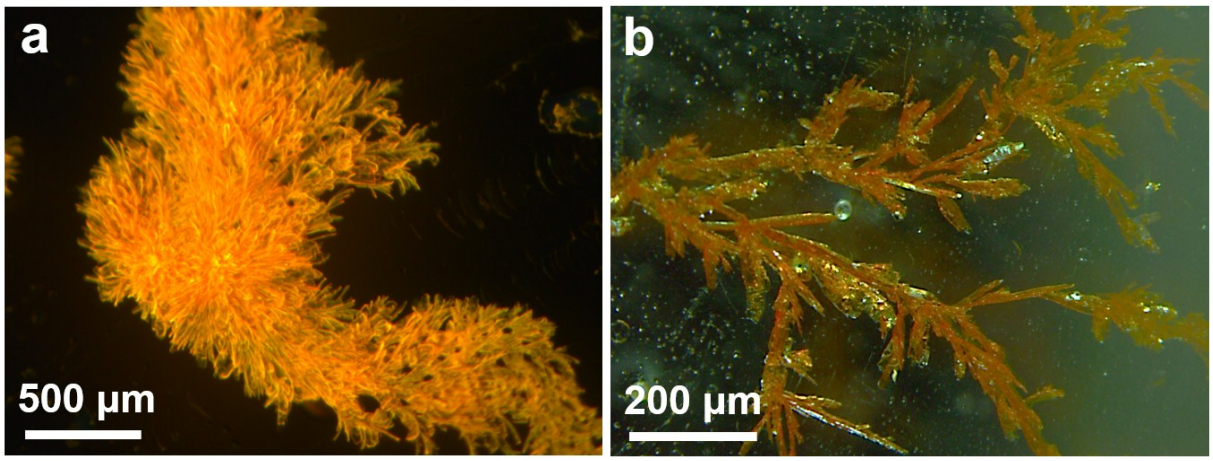

Fig. S22 Fluorescence microscopy images of BTD-TPA crystals at low magnification (a) and high magnification (b).

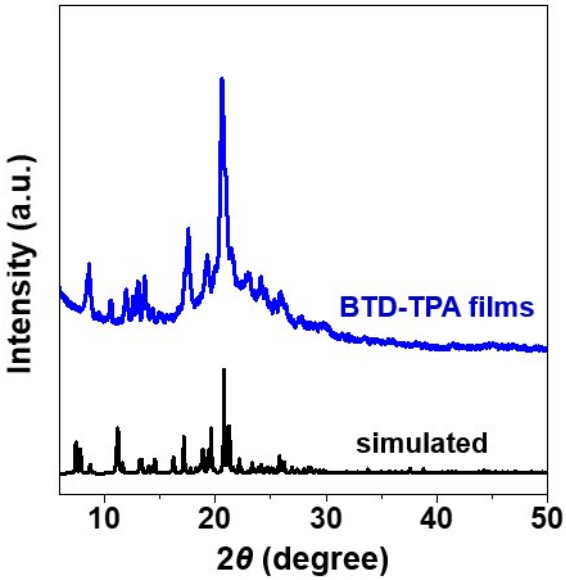

Fig. S23 XRD pattern of BTD-TPA films.

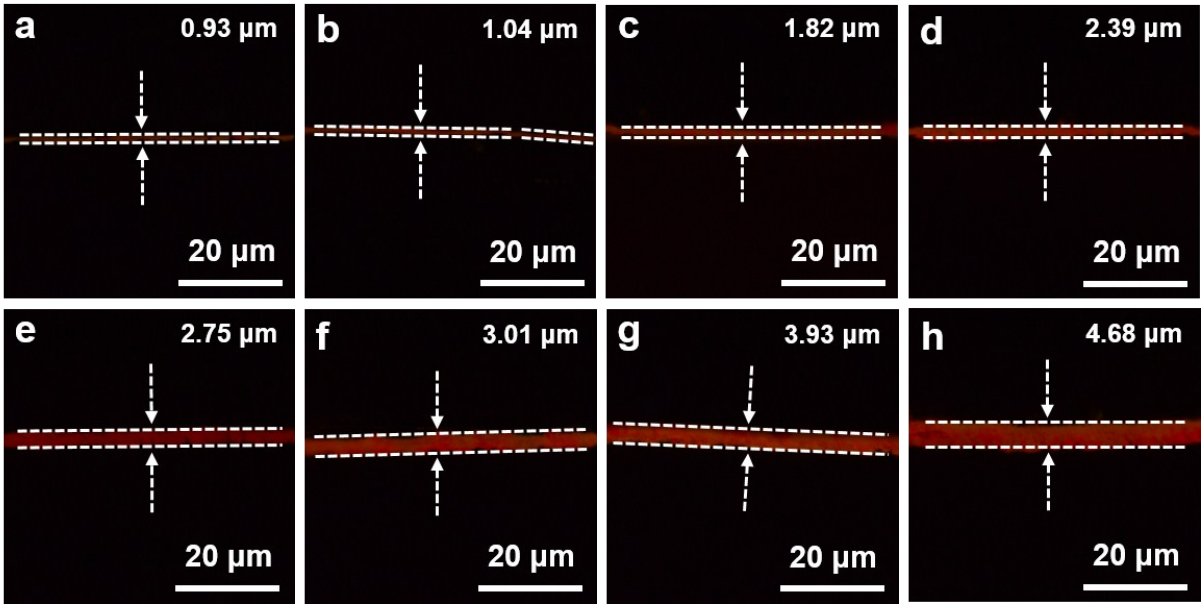

Fig. S24 Fluorescence microscopy images of BTD-TPA films on Au wafers at loadings of (a) 26 ng/mm^2, (b) 52 ng/mm^2, (c) 104 ng/mm^2, (d) 208 ng/mm^2, (e) 260 ng/mm^2, (f) 312 ng/mm^2, (g) 416 ng/mm^2, and (h) 520 ng/mm^2.

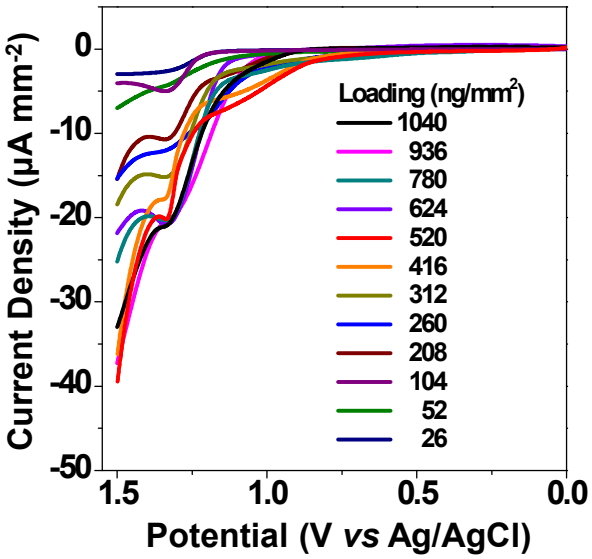

Fig. S25 LSV curves of BTD-TPA film at different loadings on Au wafers in 0.2 M PBS solutions. pH = 8.

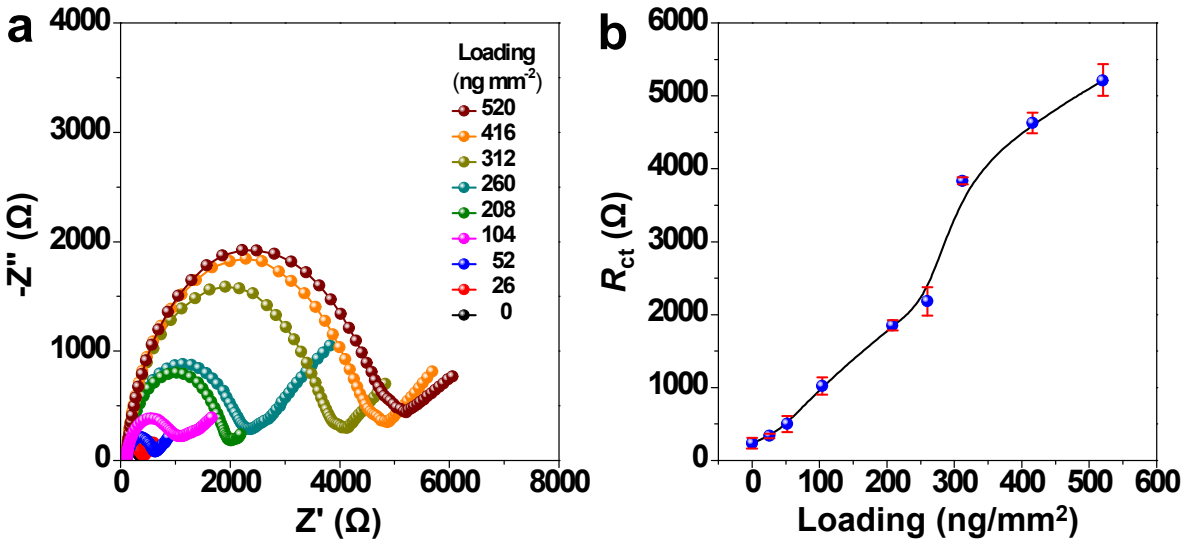

Fig. S26 (a) EIS profiles of BTD-TPA films on GCE at different loadings in 5 mM $K_3[Fe(CN)_6]/K_4[Fe(CN)_6]$ (molar ratio = 1:1) solutions containing 0.1 M KCl. (b) The plot of R_{ct} value versus BTD-TPA loading.

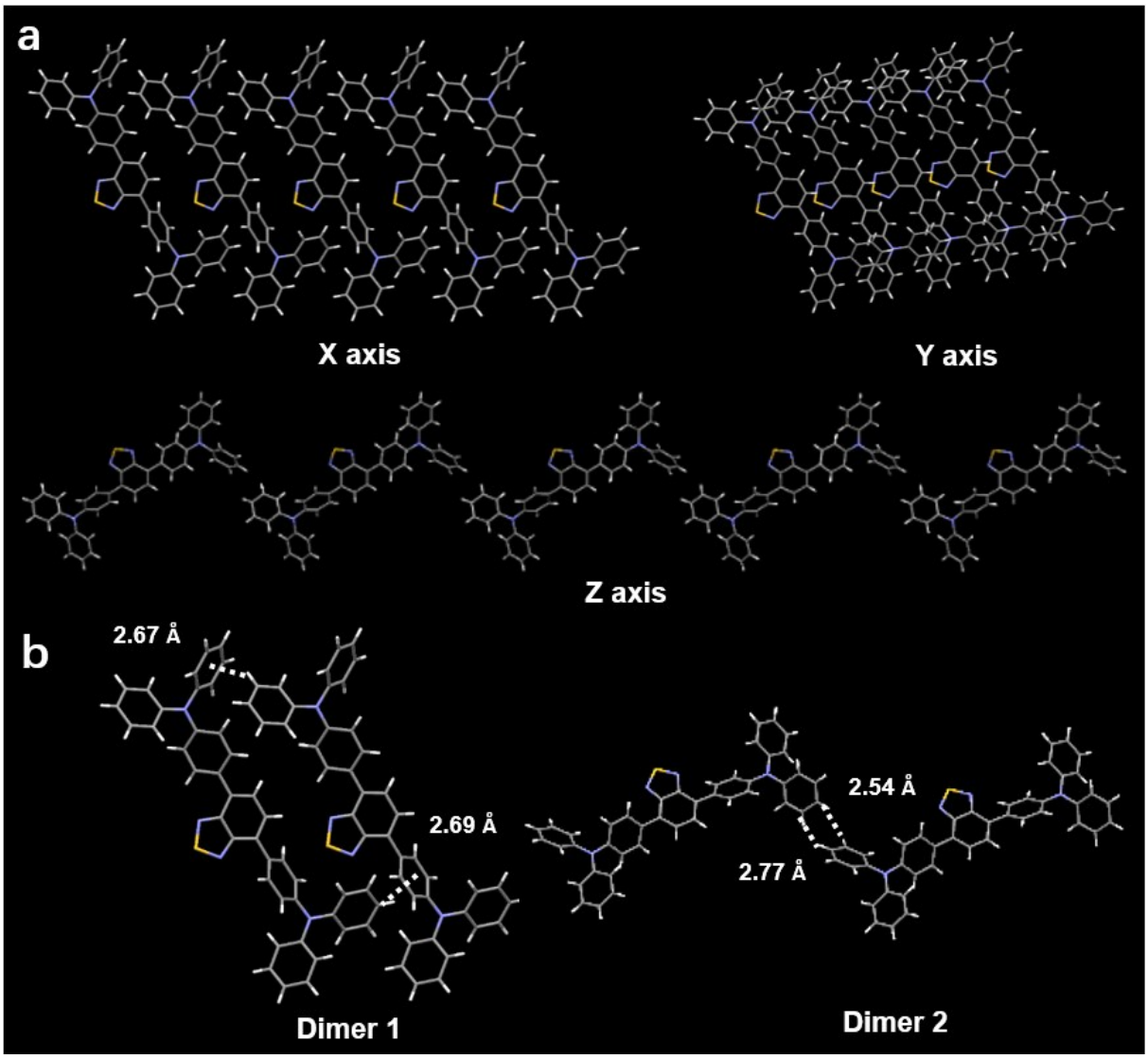

Fig. S27 Crystal structures of BTD-TPA. (a) View along X, Y, and Z axes, respectively. (b) Interaction between adjacent molecules.

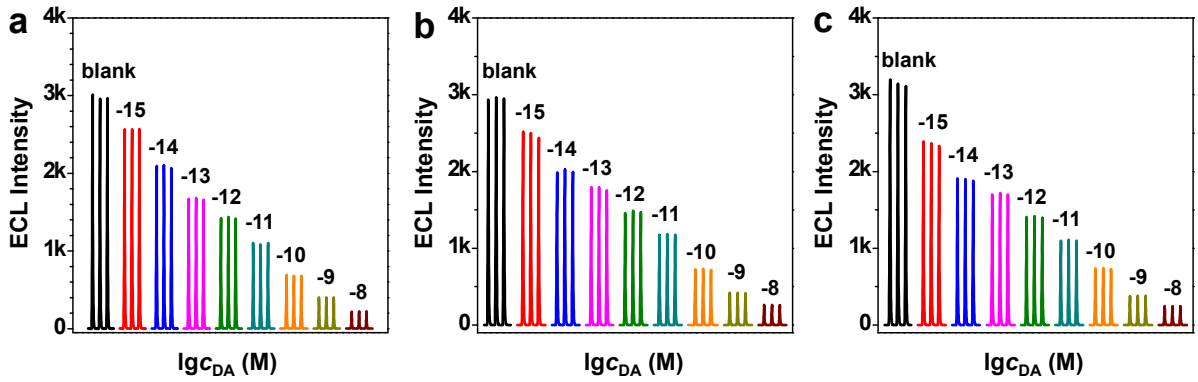

Fig. S28 ECL intensity of the BTD-TPA film (loading: 260 ng/mm^2) in the presence of various concentrations of DA. Three parallel experiments were carried out for checking reproducibility.

Table S1 Comparison of the present work with reported ECL sensors for DA detection.

Electrodes	Linear range (M)	Detection limit (M)	Reference
Cu NCs/HZ/GCE[a]	1.0×10^{-12} - 1.0×10^{-8}	3.5×10^{-13}	6
DSP-QDs/CNTs/GCE[b]	5.0×10^{-11} - 1.0×10^{-8}	2.6×10^{-11}	7
MIECLS/GCE[c]	1.0×10^{-14} - 1.0×10^{-6}	2.0×10^{-15}	8
NCD@PEI-rGO/RuNSs/GCE[d]	1.0×10^{-8} - 5.0×10^{-5}	1.0×10^{-8}	9
ZnSe/GO@MWNTs/$Ru(bpy)_3^{2+}$[e]	1.0×10^{-9} - 1.0×10^{-5}	6.0×10^{-8}	10
Au-WS_2/GE[f]	5.0×10^{-9} - 2.0×10^{-4}	3.23×10^{-9}	11
Pd NCs/GCE[g]	1.0×10^{-12} - 1.0×10^{-8}	4.6×10^{-13}	12
APTES-PTCA/GCE[h]	1.0×10^{-12} - 1.0×10^{-8}	2.9×10^{-13}	13
WO_x QDs/GCE[i]	1.0×10^{-15} - 1.0×10^{-5}	1.0×10^{-15}	14
G-CdTe QDs/TAEA-Ru/GCE[j]	1.0×10^{-14} - 1.0×10^{-9}	2.9×10^{-15}	15
MIP/QDs/AuNPs/MWCNTs/GCE[k]	1.0×10^{-14} - 2.5×10^{-12}	3.3×10^{-15}	16
BTD-TPA film/GE	**1.0×10^{-15}- 1.0×10^{-8}**	**3.3×10^{-16}**	**This work**

[a]Cu NCs/HZ: A ECL system consists of Cu nanoclusters aqueous solution and modified GCE with hydrazine. [b]DSP-QDs/CNTs: 3,3′-dithiodipropionic acid di(N-hydroxysuccinimide ester)-functionalized CdTe quantum dots/multiwalled carbon nanotubes. [c]MIECLS: A quenching-type electrochemiluminescence sensor consists of up-conversion nanoparticles, COFs-based ECL enhancement material and oligoaniline-crosslinked gold nanoparticles imprinting recognition sites. [d]NCD@PEI-rGO/RuNSs: N-doped carbon dots@poly(ethylenimine)-reduced graphene oxide/$Ru(bpy)_3^{2+}$ nanosheets. [e]ZnSe/GO@MWNTs/$Ru(bpy)_3^{2+}$: ZnSe quantum dots/graphene oxide@multiwalled carbon nanotubes/$Ru(bpy)_3^{2+}$. [f]Au-WS_2/GE: Au nanoparticles-WS_2 nanosheets/gold electrode. [g]Pd NCs: Pd nanocones. [h]APTES-PTCA: 3-aminopropyltriethoxysilane functionalized 3,4,9,10-perylenetetracar-boxylic acid. [i]WO_x QDs: tungsten oxidequantum dots. [j]G-CdTe QDs/TAEA-Ru/GCE: graphene-CdTe quantum dots/selfenhanced Ru(II) composite. [k]MIP/QDs/AuNPs/MWCNTs/GCE: molecularly imprinted polymer/CdSeTe/ZnS QDs/Au nanoparticles/multiwalled carbon nanotubes.

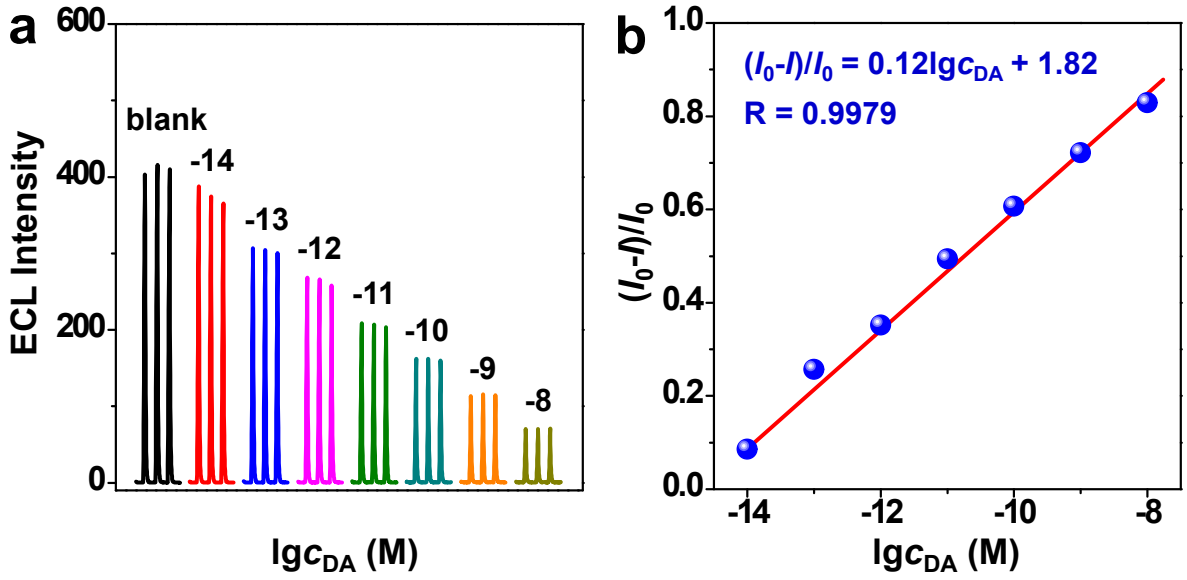

Fig. S29 (a) ECL intensity of the BTD-TPA film (loading: 52 ng/mm^2) in the presence of various concentrations of DA. (b) The plot of $(I_0\text{-}I)/I_0$ value against logarithm of DA concentration.

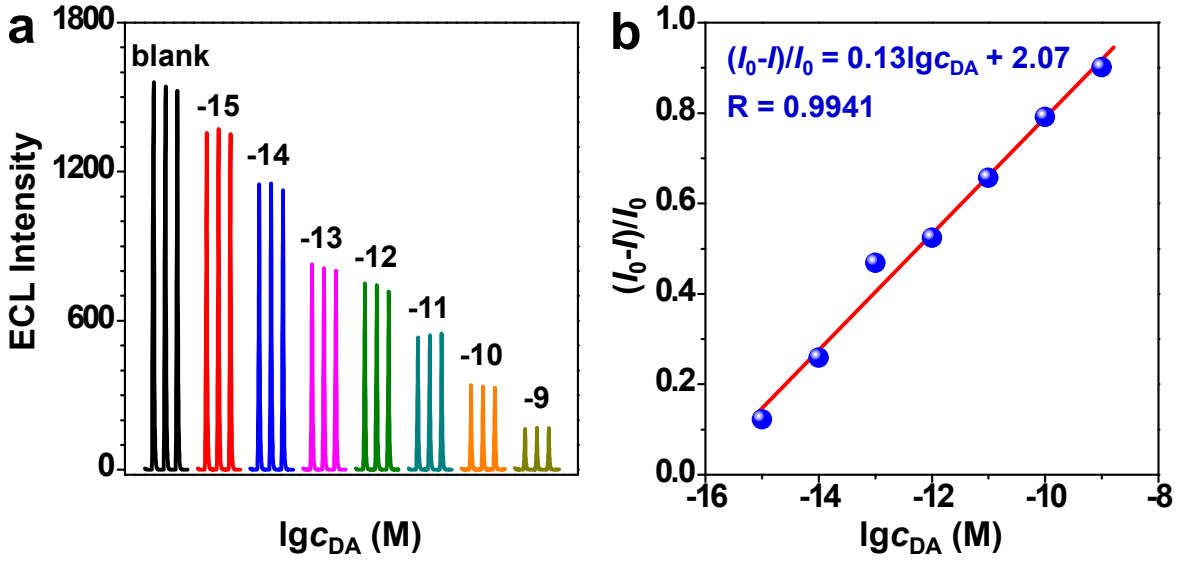

Fig. S30 (a) ECL intensity of the BTD-TPA film (loading: 208 ng/mm^2) in the presence of various concentrations of DA. (b) The plot of $(I_0\text{-}I)/I_0$ value against logarithm of DA concentration.

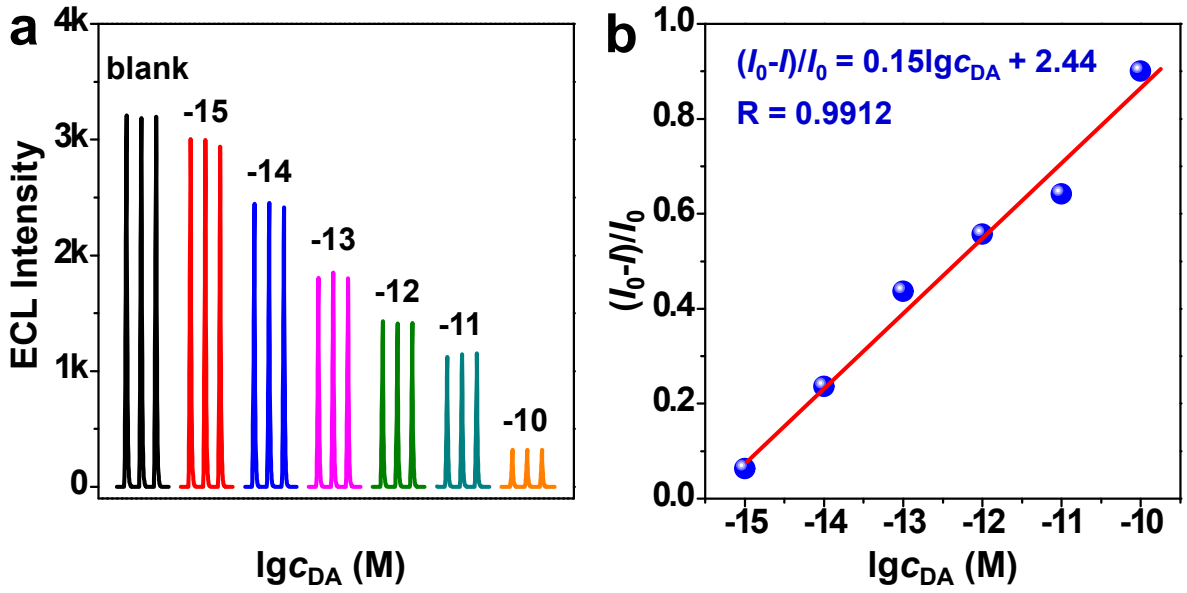

Fig. S31 (a) ECL intensity of the BTD-TPA film (loading: 312 ng/mm^2) in the presence of various concentrations of DA. (b) The plot of $(I_0\text{-}I)/I_0$ value against logarithm of DA concentration.

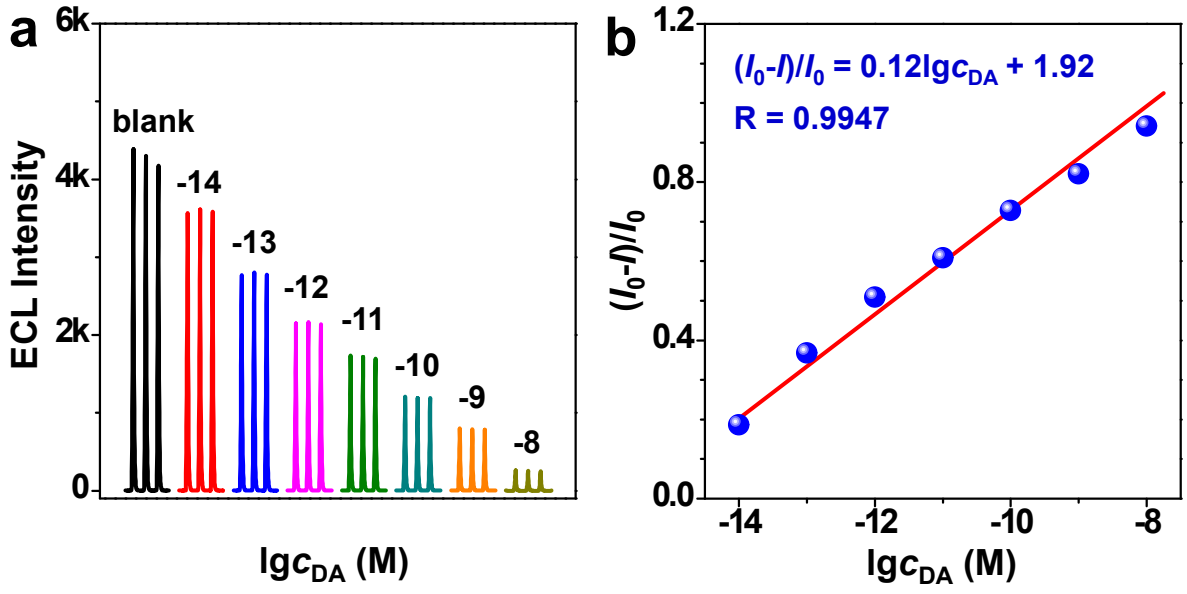

Fig. S32 (a) ECL intensity of the BTD-TPA film (loading: 416 ng/mm^2) in the presence of various concentrations of DA. (b) The plot of $(I_0\text{-}I)/I_0$ value against the logarithm of DA concentration.

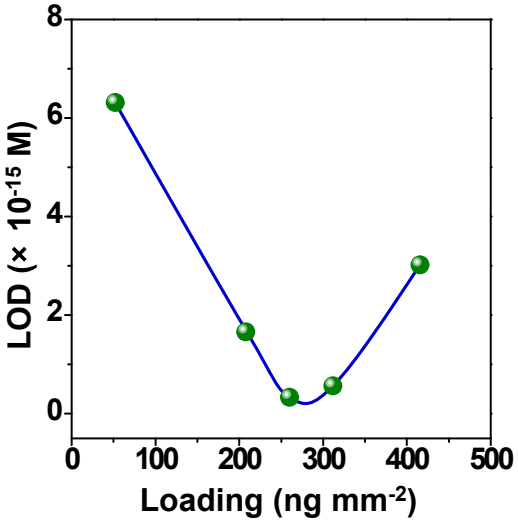

Fig. S33 The plot of limit of detection (LOD) versus luminogen loading.

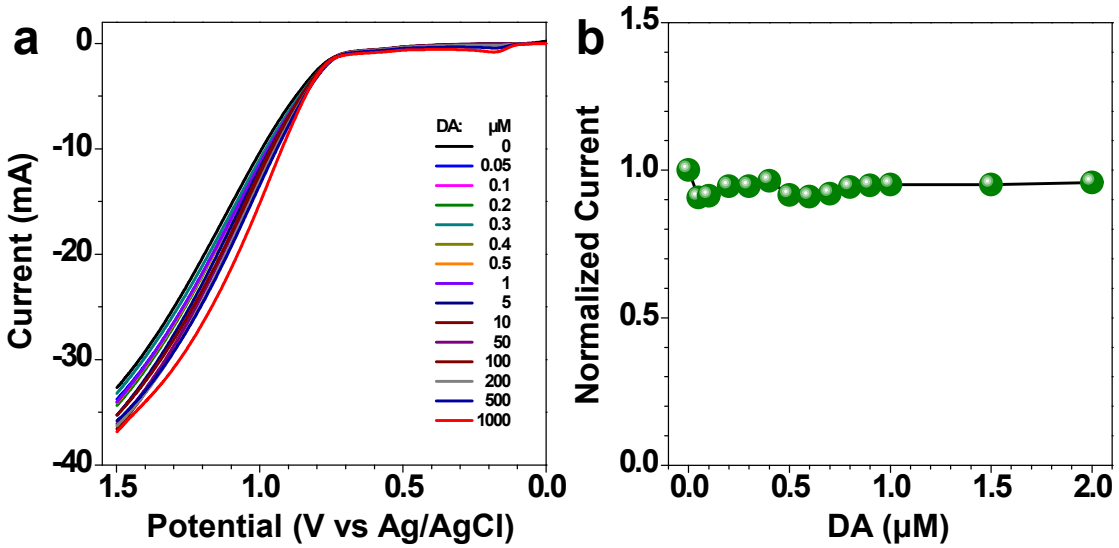

Fig. S34 (a) LSVs of BTD-TPA films in 0.2 M PBS containing different concentrations of DA. Scan rate: 0.1 V/s. (b) The plot of relative current (I_0/I) versus the concentration of DA. I_0 denotes the current of BTD-TPA films in the absence of DA.

ECL of the film is almost quenched in the presence of 10^{-8} M of DA (Fig. 6). Change in current of the film during ECL process was monitored in the presence of DA up to 1 mM, 5 orders of magnitude than the concentration required to quench ECL.

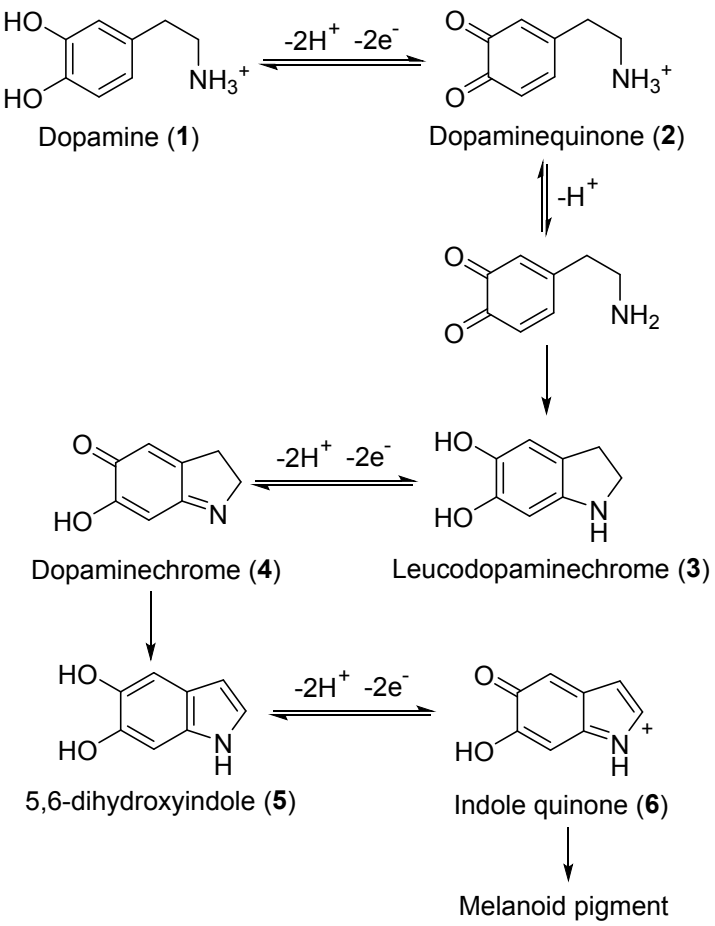

Fig. S35 Oxidation of dopamine.

Dopamine undergoes a series of reactions during electrochemical oxidation. Its reaction pathway is summarized in Fig. S35 [17-19]. Following the facile two-electron oxidation of dopamine (**1**) to dopamine-oquinone (**2**), ring closure via deprotonation of the amine side chain to leucodopaminechrome (5,6-dihydroxyindoline,**3**) occurs irreversibly. Compound **3** is then oxidized to dopaminechrome (**4**), which rearranges to 5,6-dihydroxyindole (**5**). Compound **5** is further oxidized to indole quinone (**6**), which begins the polymerization process.

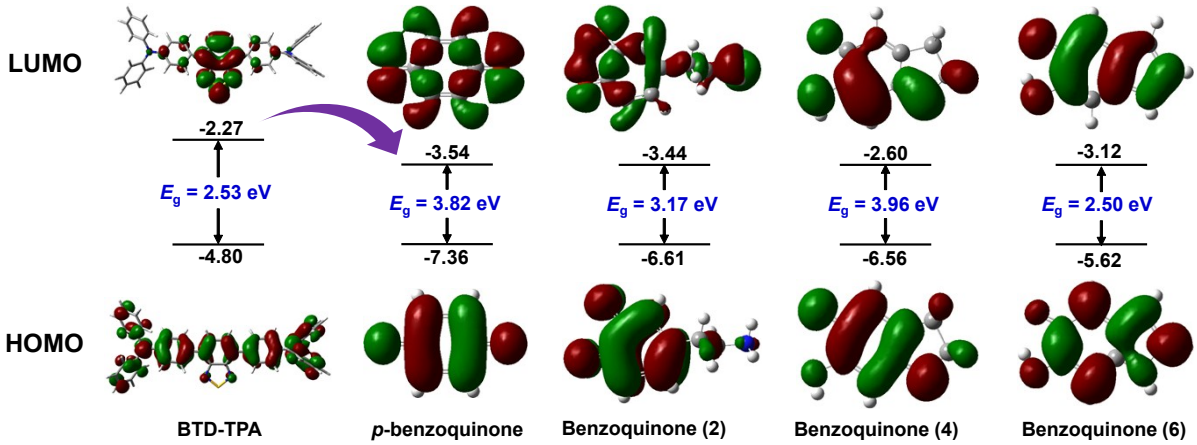

Fig. S36 Energy levels, energy gaps and molecular orbitals of the HOMO and LUMO of BTD-TPA, *p*-benzoquinone, and oxidized species of DA calculated by B3LYP/6-31+(d) program.

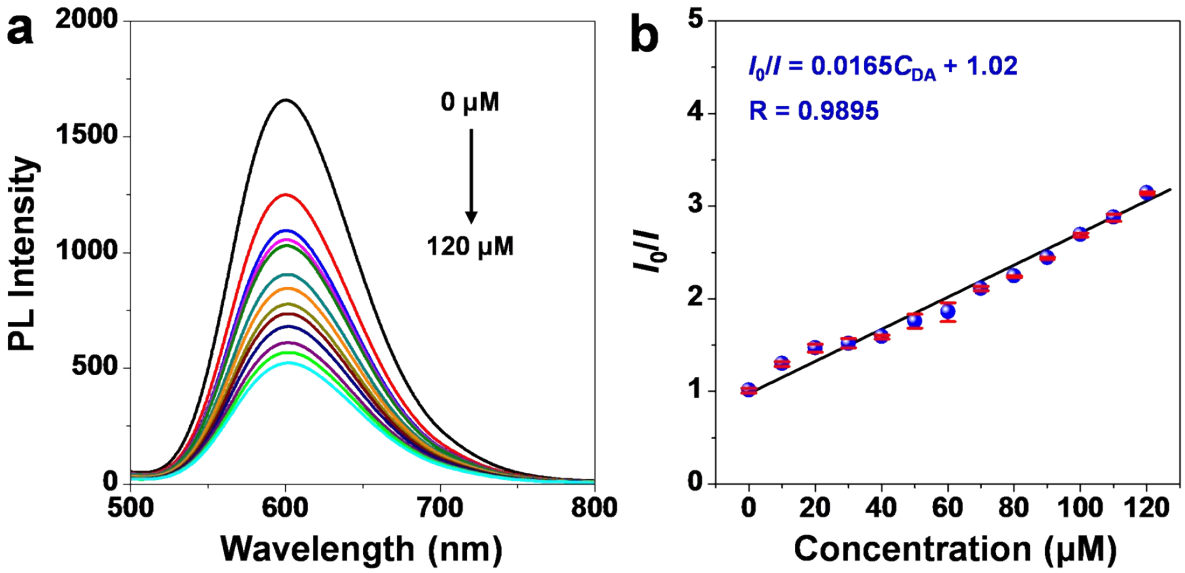

Fig. S37 (a) PL spectra of BTD-TPA containing different concentrations of *p*-benzoquinone. (b) Plots of the relative PL intensity (I_0/I) of BTD-TPA in THF solution versus concentration of *p*-benzoquinone. Luminogen concentration: 10 μM; λ_{ex} = 460 nm.

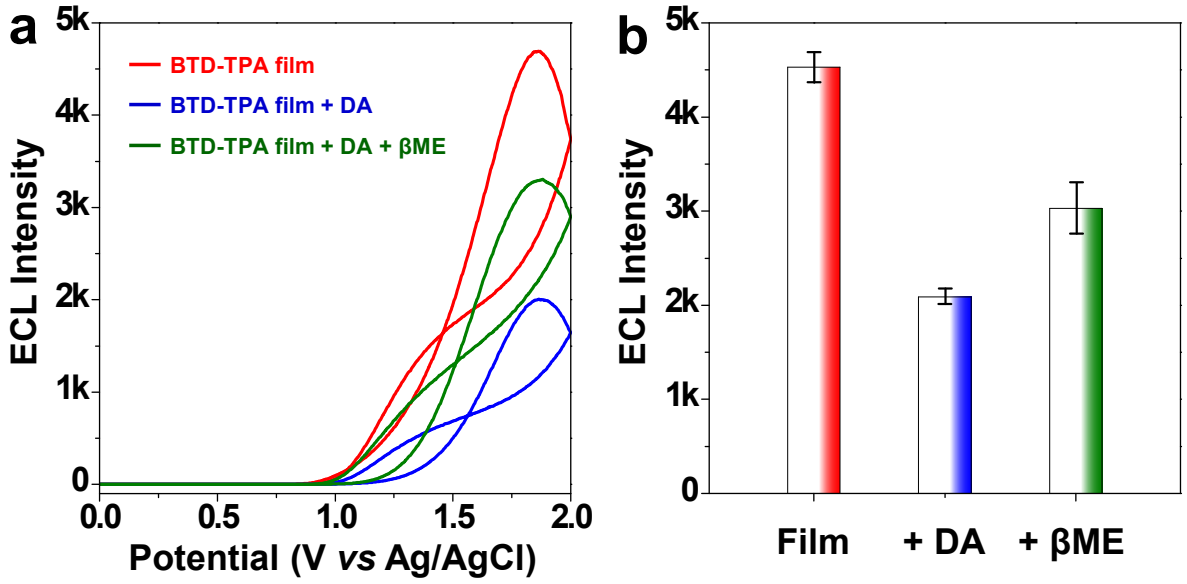

Fig. S38 (a) ECL-potential profiles and (b) ECL intensity of the BTD-TPA film, with 1 nM of DA, with 1 nM of DA and 20 nM of 2-mercapoethanol (βME).

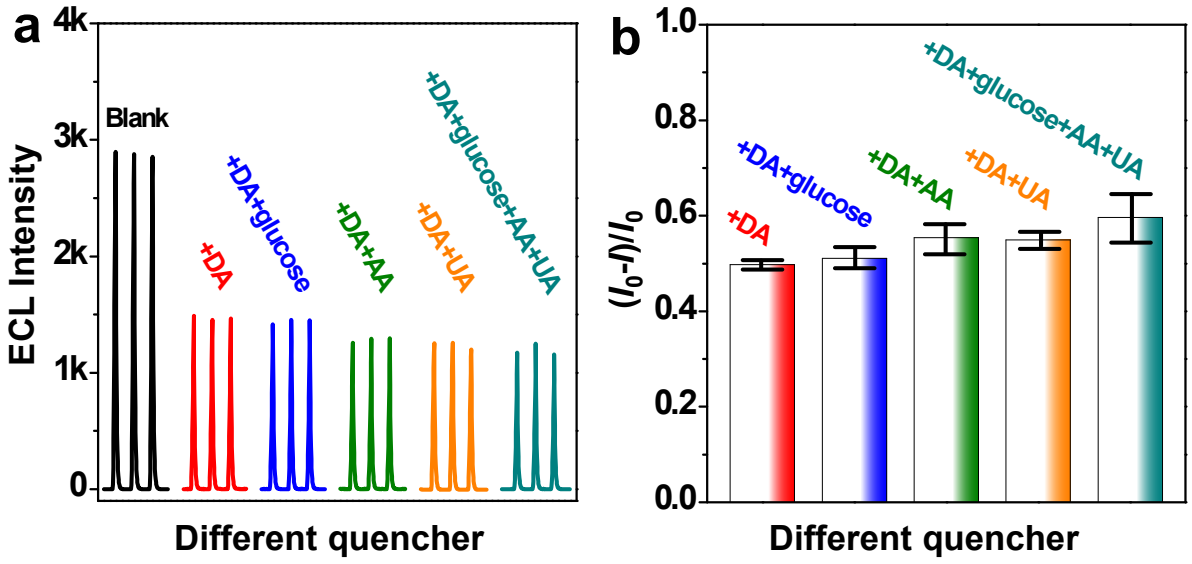

Fig. S39 ECL-potential profiles (a), and (b) $(I_0\text{-}I)/I_0$ of the BTD-TPA film with 1 pM of DA containing 1000-fold concentrations of AA, UA and glucose. Luminogen loading was 260 ng/mm^2.

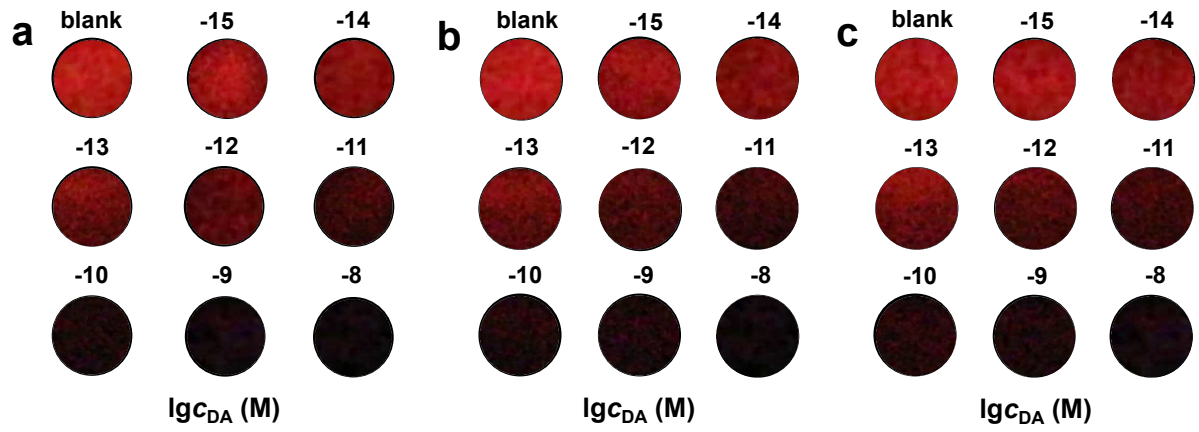

Fig. S40 ECL images of BTD-TPA films in the presence of various concentrations of DA. Three parallel experiments were carried out for checking reproducibility.

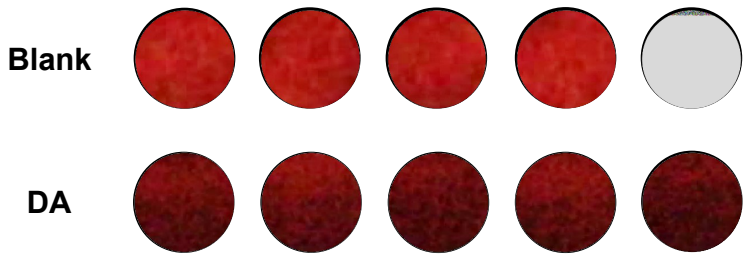

Fig. S41 ECL images of BTD-TPA films in the absence and presence of DA (2×10^{-12} M). Five parallel experiments were carried out for checking reproducibility.

Table S2 Grayscale analysis data of the ECL film.

	Grayscale	**Average value**	G_0-G/G_0	c_{DA} ($\times 10^{-12}$ M)	**Relative error (%)**
blank	27.6, 26.8, 25.4, 25.6, 24.4	26.0 ± 1.2	0.48 ± 0.08	2.04 ± 1.50	2
with DA (2×10^{-12} M)	11.3, 12.4, 13.5, 14.7, 14.9	13.4 ± 1.5			

References

1. S. i. Kato, T. Matsumoto, T. Ishi i, T. Thiemann, M. Shigeiwa, H. Gorohmaru, S. Maeda, Y. Yamashita and S. Mataka, *Chem. Commun.*, 2004, 2342–2343.
2. J. Suk, Z. Wu, L. Wang and A. J. Bard, *J Am Chem Soc*, 2011, **133**, 14675–14685.
3. W. Qin, D. Ding, J. Liu, W. Z. Yuan, Y. Hu, B. Liu and B. Z. Tang, *Adv. Funct. Mater.*, 2012, **22**, 771–779.
4. Z. Han, Z. Yang, H. Sun, Y. Xu, X. Ma, D. Shan, J. Chen, S. Huo, Z. Zhang, P. Du and X. Lu, *Angew. Chem.*, 2019, **131**, 5976–5980.
5. K. N. Swanick, S. Ladouceur, E. Zysman-Colman and Z. Ding, *Chem Commun (Camb)*, 2012, **48**, 3179–3181.
6. M. Zhao, A. Y. Chen, D. Huang, Y. Zhuo, Y. Q. Chai and R. Yuan, *Anal. Chem.*, 2016, **88**, 11527–11532.
7. L. Zhang, Y. Cheng, J. Lei, Y. Liu, Q. Hao and H. Ju, *Anal. Chem.*, 2013, **85**, 8001–8007.
8. Y. Gu, J. Wang, H. Shi, M. Pan, B. Liu, G. Fang and S. Wang, *Biosens. Bioelectron.*, 2019, **128**, 129–136.
9. L. Li, D. Liu, H. Mao and T. You, *Biosens. Bioelectron.*, 2017, **89**, 489–495.
10. L. Tian, X. Wang, K. Wu, Y. Hu, Y. Wang and J. Lu, *Sensor Actuat. B-Chem.*, 2019, **286**, 266–271.
11. Z. Wang, X. Wang, X. Zhu, J. Lv, J. Zhang, Q. Zhu and Z. Dai, *Sensor Actuat. B-Chem.*, 2019, **285**, 438–444.
12. H. M. Wang, C. C. Wang, A. J. Wang, L. Zhang, X. Luo, P. X. Yuan and J. J. Feng, *Sensor Actuat. B-Chem.*, 2019, **281**, 588–594.
13. X. Fu, Y. Yang, N. Wang and S. Chen, *Sensor Actuat. B-Chem.*, 2017, **250**, 584–590.
14. H. Peng, P. Liu, W. Wu, W. Chen, X. Meng, X. Lin and A. Liu, *Anal. Chim. Acta*, 2019, **1065**, 21–28.
15. X. Fu, X. Tan, R. Yuan and S. Chen, *Biosens. Bioelectron.*, 2017, **90**, 61–68.

16. Z. Wang, Y. Qian, X. Wei, Y. Zhang, G. Wu and X. Lu, *Electrochim. Acta*, 2017, **250**, 309-319.

17. M. Hawley, S. Tatawawadi, S. Piekarski and R. N. Adams, *J. Am. Chem. Soc.*, 1967, **89**, 447-450.

18. T. E. Young and B. W. Babbitt, *J. Org. Chem.*, 1983, **48**, 562-566.

19. H. Muguruma, Y. Inoue, H. Inoue and T. Ohsawa, *J. Phys. Chem. C*, 2016, **120**, 12284-12292.